Calibration of RFI Detection Levels in a Low-Cost GNSS Monitor

Nicolas Roberto San Miguel
Stanford University
Stanford, USA
nicolas6@stanford.edu

Yu-Hsuan Chen
Stanford University
Stanford, USA
yuhsuan.chen@stanford.edu

Sherman Lo
Stanford University
Stanford, USA
sherman.lo@stanford.edu

Todd Walter
Stanford University
Stanford, USA
twalter@stanford.edu

Dennis Akos
University of Colorado, Boulder
Boulder, USA
dma@colorado.edu

***Abstract*—The Global Navigation Satellite Systems (GNSS) is an invaluable tool that is heavily used in everyday life across numerous industries. Despite their ubiquitous use, GNSS signals are very vulnerable to both intentional and unintentional forms of radio frequency interference (RFI). This paper supports the development of a low-cost GNSS RFI monitor that can reliably enhance a user's spatial awareness with respect to the state of RFI in their local environment. Multiple jamming experiments are conducted using an anechoic chamber to analyze the response of three different receivers to both wideband and narrowband forms of jamming. The power level of the jamming signal is varied to show how changes affect recorded metrics in the receiver. Specifically, the automatic gain control (AGC), the carrier-to-noise power density ratio (CN0), spectrum, and position information are valuable in understanding the receiver's state. These results provide a reference for calibrating low-cost receivers when monitoring for interference.**

***Index Terms*—GNSS, RFI, Low-Cost Monitor, u-blox, AGC**

I. Introduction

Global Navigation Satellite Systems (GNSS) are integral to numerous industries and commercial products. Aviation, defense, shipping, and agriculture among others heavily rely on GNSS measurements to provide positioning information accurately and reliably. However, GNSS signals are vulnerable to both intentional and unintentional radio frequency interference (RFI). RFI typically comes in the form of jamming which seeks to deny the use of healthy GNSS signals. However, it can come in a more pernicious form, spoofing, which seeks to relay incorrect positioning information to a user. Because GNSS is used in so many day-to-day applications, developing a low-cost method of detecting and understanding interference for a user and within their local environment is increasingly important. Multiple low-cost monitors distributed over a local environment could provide a user with spatial awareness to the presence of RFI in a given area. A future goal would be for these monitors to help classify and even localize the RFI.

This work was supported by the Aerospace Corporation through their University Partnership Program and by the Federal Aviation Administration.

II. Background and Motivation

A. RFI Events

RFI events are becoming increasingly commonplace and can seriously affect civilian airspace. In 2022, interference events disrupted traffic at two major US airports, and the sources remain unsolved [1], [2]. However, the threats of interference extend far beyond disrupting traffic and can severely affect safety-critical systems [3]. Thus, there is a strong need to be able to detect, localize, and stop the source of interference quickly. Stopping means not just providing location but also supporting evidence (in the form of performance metric changes, spectrum analysis, etc.) to the authorities who can act on the problem and prosecute the offending party.

B. Existing Reference Receivers

The most common way of detecting interference is with ground based reference receivers, and traditionally, high end reference receivers have been examined. High-end receivers are generally effective at handling RFI individually and use proprietary software to filter and mitigate interference internally. However, large scale usage of such receivers is impractical due to equipment and maintenance/security costs of multiple receiver units. There are high-end receivers operated as part of other systems, such as those in the Wide Area Augmentation System (WAAS), that can contribute to RFI monitoring. While it is true that existing receivers such as those that make up WAAS can contribute to monitoring, any such low-density ground-borne solution will suffer from line of sight limitations and will consequently have large observation gaps. The line of sight (LOS) limitation is an important issue when using high end reference receivers since they are generally too expensive to deploy widely or in high density, but a low-cost receiver will allow for greater density at a comparable or lower cost. Other solutions include using spaceborne receivers as they can overcome the line of sight limitations seen with ground based monitoring. There has been some use of GNSS receivers on the International Space Station and other low earth orbiting assets to perform RFI detection.

However, these assets are both hard to acquire and not as sensitive due to their much greater distance to suspected RFI sources.

Having a broad deployment of low-cost monitors mitigates the limitations of the two methods discussed above and forms an integrated solution with tiers of information (ground, airborne, and space-based monitors) to be able to detect RFI reliably and provide evidence needed to prosecute the offender. A low-cost monitor allows for wide spread deployment which then increases coverage area compared to using high-end reference receivers alone. The monitor is also closer to the interference source which allows for better sensitivity and characterization. Importantly, a low-cost monitor can integrate with both ground-based augmentation and spaceborne systems, providing features that complete these other detection methods.

Hence, this paper focuses on low-cost ground-based monitors and its capabilities as an essential step to an overall interference detection and localization (IDL) strategy.

C. Low-Cost Monitor

To develop a system to detect and localize interference requires receivers capable of monitoring GNSS signals for interference. High end receivers have many features and capabilities for IDL; however, they are limited in quantity by their cost. To meaningfully have this capability, many monitors that are spread across a local area are required to service that environment, and consequently (particularly for a ground-based system), these receivers must be low-cost.

GNSS receivers can have many features and capabilities (high sensitivity, spectrum analysis, adaptive noise monitoring) that can enhance IDL. Some features are only seen on high end receivers while other features are can be found in mass market receivers. For example, features such as high sensitivity may even be more common on low-cost, mass market receivers than the highest end survey receivers. Since some RFI mitigation features may make the interference less visible, there is a tradeoff between sensitivity to and robustness against interference. Thus, it is important to see and characterize the response of different potential monitor receivers to understand how to use them for reliable RFI detection. This paper explores the tradeoffs when using different classes of receivers for developing a RFI monitor suitable for mass deployment. This work builds on previous work to develop a low-cost GNSS RFI monitor [4], [5] which has explored features of a low-cost receiver and its sensitivity to interference. To explore the tradeoffs between low-cost models and higher-cost models in the presence of controlled RFI, we examine the performance of receivers in various classes under the same RFI conditions.

Interest in developing a low-cost monitor has been explored in [6] as well. These projects build on a larger body of work that describes how different types of RFI affect receiver metrics, specifically the effects of low-cost front-end components on detection [7] and the effects on various power and signal quality metrics [8], [9]. Additionally, generalized frameworks have been explored both for RFI detection and for combining metrics in networked receivers [10], [11].

III. Test Design and Metrics

Three different receivers and antennas are tested to consider the effects of each on recorded metrics. The receivers consist of low-cost, medium-cost, and high-cost models while the antennas include of a commercial-grade, survey-grade, and aviation-grade models. Data is recorded from each receiver and processed in MATLAB.

A. Test Receivers

Three different receivers are tested to compare differences in each type. All of the evaluated receivers measure basic metrics (CN0, number of satellites, etc.); however, they differ slightly in how they record power metrics such as AGC and programmable gain amplifier (PGA) gain. Each receiver varies in cost and complexity to compare the relative performance of different models. The lowest-cost receiver is the u-blox ZED-F9T-10B [12], with multi-constellation, multi-frequency (L1/L5/E5a) data. The tracking and navigation sensitivity is -167 dBm and the signals tracked include the following: GPS L1C/A, L5, GLONASS L1OF, Galileo E1 B/C, E5a, BeiDou B1I, B1C, B2a, QZSS L1C/A, L5, SBAS L1C/A, and WAAS. There is a stated CW detection capability and on-board band pass filters.

The more expensive Septentrio mosaic-X5 [13] is a low-power multi-constellation, multi-frequency (L1/L2/L5) receiver with 448 channels which tracks the same signals as the u-blox but additionally GPS L1PY, L2C, L2P, GLONASS L1CA, L2P, L3 CDMA, Galileo E5b, E5AltBOC, and QZSS L2C, L5, SBAS, and WAAS. The stated tracking performance as a CN0 threshold is given as 20 dB-Hz for tracking and 33 dB-Hz for acquisition. Also, there is interference monitoring technology for narrow/wideband and chirp RFI.

The most expensive Trimble BX940 [14] has on-board MEMS inertial sensors and tracks the following signals: GPS L1C/A, L2E, L2C, L5, GLONASS L1C/A, L2C/A, L3 CDMA, Galileo E1, E5a, E5b, E5AltBOC, BeiDou B1, B2, QZSS L1C/A, L2C, L5, and SBAS L1C/A, L5. Interference detection consists of on-board RF Spectrum Analysis.

All three receivers have proprietary on-board interference detection and mitigation software of some form. Details about this internal filtering in the u-blox receiver specifically was previously explored in [5]. The more costly receivers contain more sophisticated filtering and detection software, and BX940 receiver is made more expensive by the integrated inertial sensors.

Details specific to each receiver are described in Table I.

B. Test Antennas

Additionally, three different antennas are compared to evaluate the effects of RFI on each receiver when the antenna is varied.

The first antenna tested is a u-blox ANN-MB1 L1/L5 patch antenna. This is an active antenna with an low-noise amplifier

TABLE I: Receiver Comparison

Receiver	Metric Comparison			
	Relative Cost	***Tracking Channels***	***Number of Signals***	***AGC Outputs***
u-blox F9T-10B	$	184	17	2
Septentrio mosaic-X5	$$	448	24	6
Trimble BX940	$$$	336	22	None

(LNA) gain of 29 ± 3.0 dB, an LNA noise figure of 2.7 dB, and a total gain of 22 dB [15]. The L1 band supported ranges from 1559-1606 MHz. After the patch antenna element, the amplifier architecture consists of two separate LNA and SAW components for the L1 and L5 bands, which are then combined with a single LNA for both bands before being passed into the analog-to-digital converter (ADC). The second antenna used is the Trimble Zephyr 2 Geodetic which has an overall gain of 50 dB with an integral LNA and out-of-band rejection [16]. The third antenna is a Sensor Systems S67-1575-175 aviation antenna that is designed for the GPS L1/L5 bands. It is a passive antenna and features special filtering for aviation applications [17].

A comparison of the antennas is included in Table II.

TABLE II: Antenna Comparison

Antenna	Metric Comparison		
	Type	***Overall Gain [dB]***	***Type***
ANN-MB1 u-blox antenna	commercial	22	active
Trimble Zephyr 2 Geodetic	survey	50	active
Sensor Systems S67-1575-175	aviation	0	passive

C. Data Recording

The u-blox receiver records data in the form of a .ubx message, which is recorded using u-center software. The .ubx data file is then transferred to MATLAB where it is parsed into individual messages containing a variety of metrics and is analyzed. Among the numerous available metrics, ones of particular interest are those that describe signal quality and receiver status such as the carrier-to-noise power density (CN0) and the automatic gain control (AGC). Additionally, frequency spectrum information is particularly useful for analysis.

The Septentrio receiver records into .sbf files which are unpacked and converted to MATLAB as well. In addition to the standard signal quality metrics and raw GNSS measurements, the Septentrio also records more precise AGC and spectrum information than the u-blox. The Trimble receiver similarly records all the standard metrics however it does not record AGC.

D. Defining RFI Levels

We seek to identify for a given receiver, at what point interference is detectable (compared to noise in nominal conditions) and at what point interference is overpowering (based on degrading the metrics that contribute to the position solution). To do this we compare observed results against values observed in nominal data. A threshold is defined using the standard deviation of nominal data and can be adjusted based on the user's desired sensitivity. For an initial evaluation, the threshold is set to be $\pm 2\sigma$ of the mean values recorded in the nominal data.

IV. Experimental Methods

First, we discuss the nominal data collection method, its motivation, and its limitations. Then we discuss the jamming scenarios.

A. Nominal Data

We explore the point at which jamming becomes distinguishable from nominal conditions. For this, a u-blox F9T-10B receiver is run for 30 days at the Stanford GPS Lab to collect nominal data. The setup has an open sky field of view, reducing multipath interference, and is in a suburban environment, reducing instances of interference from highways or urban areas [18]. Despite being relatively clean, this data is not completely clean, as it contains small instances of interference attributed to sporadic RFI sources.

There is difficulty in defining what is a 'nominal' state. When starting to record data it is assumed that there is no interference present; however, it is hard to say with certainty that no RFI is present without comparing against known information of what defines nominal operation. To mitigate the influence of instances of RFI in the nominal data collection, we average data over 30 days (2.6e6 seconds).

Nominal data is collected using a commercial u-blox antenna (ANN-MB1) and is recorded and uploaded daily to a central server. Results are summarized in Table III.

B. Jamming Experiment Design

The experimental setup consists of an anechoic chamber which is used to transmit jamming signals in the presence of live, rebroadcasted GNSS signals. The jamming signals are computer-generated and is re-played through a USRP B200 mini software-defined radio (SDR) and is broadcast inside the anechoic chamber. Live GNSS signals are collected on the roof of the Durand building (Stanford Department of Aeronautics and Astronautics) using a survey-grade antenna, Trimble Zephyr 2 Geodetic, and are re-broadcasted using a helical antenna inside the chamber.

Three different antennas are used to receive the signals in the chamber which are then split using an RF splitter/combiner. Only one antenna is used at a time and the output signal is split to the three receivers. The experiment is repeated three times to use each antenna with all three receivers. A block diagram visualization of the setup is included in Fig. 1 along with the three antennas and three receivers used in the tests.

The jamming signal in both cases is transmitted using a passive marine antenna also located inside the chamber. The

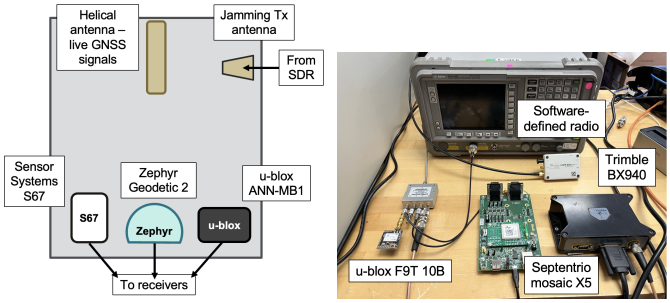

Fig. 1: Block diagram of the anechoic chamber setup (left) and the receivers used in the experiment (right).

jamming dataset is re-played through the SDR located outside the chamber. The receiving antenna signal exits the chamber and is split using a coaxial ZA4PD-2-S+ power splitter that has a range of 1000-2000 MHz. Each split signal then has a DC block to protect the individual receivers from damage.

C. Scenario Design

To analyze a range of possible RFI events, we test two basic cases: narrowband and wideband interference. The power levels of the jamming signals are chosen such that at lower levels, the GNSS signals are received as they would be nominally, and at the higher levels, significant RFI would be visible. In each jamming case, we operate the jamming signal for 2 minutes and sample at a rate of 1 Hz.

1) Narrowband Jamming: The first scenario consists of a continuous-wave (CW) jamming signal injected at the GPS L1C/A center frequency with a bandwidth of 1 MHz (1575.42 ± 0.5 MHz). A spectrum plot of CW interference is included in Fig. 2. The gain of the interference signal is varied from 25 dB to 80 dB in 5 dB increments. The 25 and 80 dB are selected because the former will still show near-nominal performance and the latter will be sufficient to completely degrade measurements on the u-blox receiver. The gains of the jamming signal are converted to measurements of power, so the range 25 to 80 dB encompass jamming signal power from -82.5 to -27.5 dBm. Each spectrum plot shows the frequency on the y-axis over a 120 second time period. The color corresponds to the distribution of power over the frequency spectrum at each time step. In the CW jamming spectrum plot, two yellow lines indicate the CW frequencies that have a higher power level than the surrounding frequencies.

2) Wideband Jamming: The additive white Gaussian noise (AWGN) jamming involves raising the noise floor over a prescribed bandwidth to drown out the true signal. This scenario is also applied to the GPS L1C/A frequency with a 40 MHz bandwidth (1575.42 ± 20 MHz). As with the CW jamming case, the jamming signal gain is varied over the same range. A visual depiction of the frequency spectrum with noise jamming is provided in Fig. 2. In the noise jamming spectrum plot, A 40 MHz wide green-yellow band indicates there is greater noise spectral density there relative to the rest of the frequency spectrum recorded by the u-blox receiver.

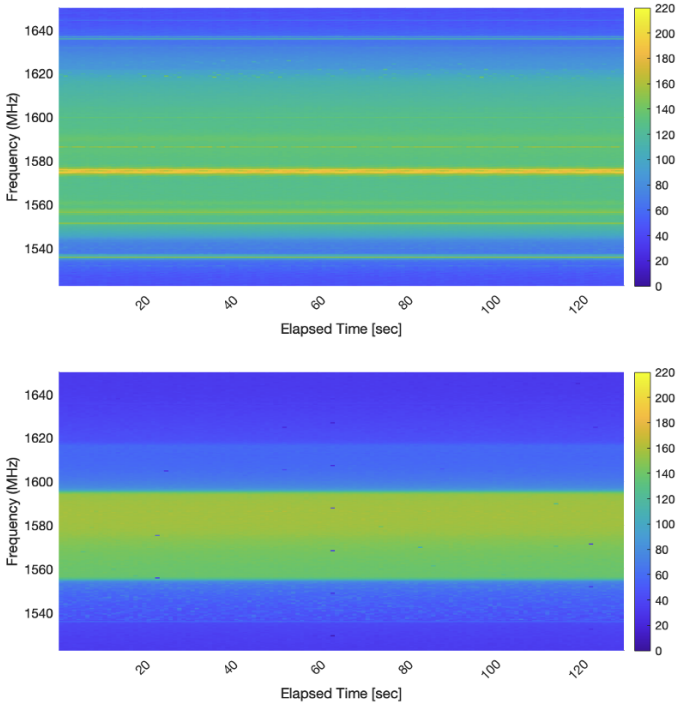

Fig. 2: Frequency spectrum (from u-blox receiver) centered at 1575.42 MHz for CW (top) and AWGN (bottom) jamming scenarios. Color scale describes the energy level relative to the rest of the frequency spectrum at each time step.

To visualize the jamming signal relative to each GNSS frequency, the diagram in Fig. 3 qualitatively overlays the narrow and wideband jamming profiles with the L1 frequencies for each major constellation. No jamming is applied to L5 frequencies. Note that the narrowband jamming is applied near GPS L1/GAL E1 frequency, but not the BeiDou B1I or GLONASS L1 frequencies. Also, the 40 MHz bandwidth AWGN jamming envelops the B1I frequency entirely but only the lower portion of the GLONASS L1 frequencies. The CW profile illustrated in 3 corresponds with the two yellow lines in 2 (top) and the AWGN jamming profile is illustrated by the green-yellow band in 2 (bottom).

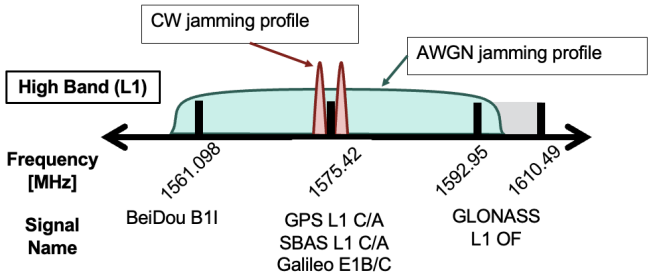

Fig. 3: L1 frequency spectrum with narrowband and wideband jamming profiles

V. Results and Analysis

First, we discuss the nominal data collection and its features. Then, we examine selected metrics for a single receiver subjected to wideband interference at varied gains. Next, cross-receiver and cross-antenna comparisons are discussed, as well as differences between the continuous wave and noise jamming scenarios in each receiver. Afterwards, the quantitative relationship between each metric and power level is described before thresholding for detection and calibration is discussed.

A. Nominal Data

The results for nominal data collection are included in Table III. The mean and standard deviation describe the spread of the time series data, while the maximum value shows the upper and lower limits of the recorded CN0 values. The maximum delta metric shows the largest change between two consecutive CN0 values.

TABLE III: Nominal Data Summary (u-blox receiver)

Metric	Statistical Measures			
	Mean	σ	***Max. Value***	***Max. delta***
Max CN0 Overall [dB Hz]	49.8	1.13	54	4
Max CN0 (GPS Only) [dB Hz]	47.9	1.06	53	3
Max CN0 (GAL Only) [dB Hz]	46.7	1.21	52	3
Max CN0 (GLO Only) [dB Hz]	48.9	1.81	54	5
AGC [%]	62.7	0.02	64.3	4.29
Number of Sats (GPS)	10.6	1.06	14	2
Number of Sats (GAL)	8.96	1.58	12	1
Number of Sats (GLO)	8.15	1.03	12	2
Horizontal position error [m]	-	0.29	1.41	0.08

B. Varied Jamming Power Levels

1) U-blox Receiver Analysis: This section includes results for performance at several jamming power levels as recorded by the u-blox receiver using the u-blox antenna. Here we present the maximum carrier-to-noise power density for GNSS satellites as well as the AGC at these jamming power levels. These results are separated by constellation in Fig. 4 and the AGC for the u-blox L1 and L5 bands are plotted in Fig. 5.

In these figures, the color intensity is associated with the jamming power level, where lighter colors indicate less power and darker colors indicate higher power. Data was collected for 12 two minute runs and compiled onto one plot to directly compare the effects of jamming power. The legends are consistent across all subsequent plots and are thus excluded for clarity. Each power level is separated by 5 dBm increments.

Fig. 4 shows the maximum CN0 recorded by each constellation at each time-step. As expected, at higher jamming power levels, the maximum CN0 value drops from 50 dBHz to near 20 dBHz for GPS and Galileo. The CW jamming signal is located near the GPS L1/GAL E1 frequency, which is why the magnitude of drops observed with those constellations are not observed with GLONASS or BeiDou, which drop to 28 dBHz and 40 dBHz, respectively. These drops are still relatively large considering the CW jamming signal is not

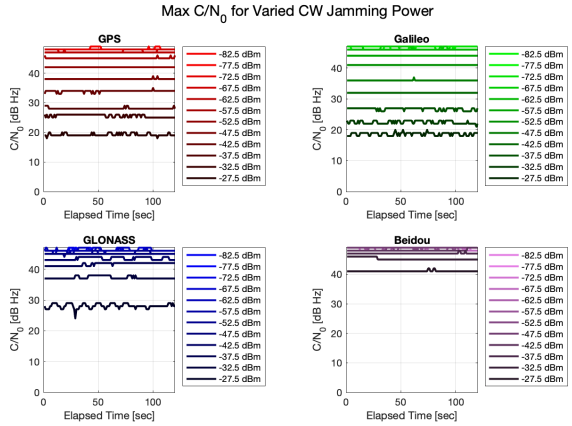

Fig. 4: Maximum CN0 for GPS, Galileo, GLONASS, and BeiDou constellations at selected CW jamming power levels (u-blox antenna, u-blox receiver).

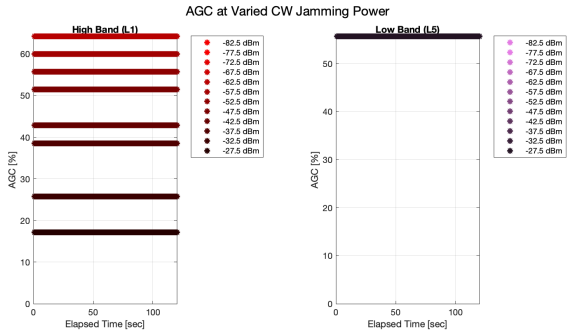

Fig. 5: U-blox AGC for L1/L5 at selected CW jamming power levels (u-blox antenna, u-blox receiver).

near the BeiDou B1I or GLONASS L1 frequencies, but these effects are discussed in the subsequent analysis. The AGC is plotted in Fig. 5, which shows an expected drop in AGC for higher jamming power. Jamming is applied only to the L1 band and no drop in AGC on the L5 band is observed. No consistent cross-frequency interference was observed across all the results.

2) Cross-Receiver Comparison: To compare differences between receivers, we look at results for jamming tests conducted with the same antenna and type of jamming. First, we compare the CW jamming results using the u-blox antenna. Fig. 6 shows the maximum CN0 over time for each constellation and receiver. The legends for these plots are the same as those for Fig. 4. In each of the three plots here, the GPS and Galileo signals drop for higher jamming power, and the step size and range of the drops vary by receiver type. The largest drops of 30 dBHz are seen with the u-blox receiver whereas drops of 25 dBHz and 10-20 dBHz are seen in the Septentrio and Trimble receivers. The smaller drops associated with the more sophisticated receivers may be the result of individual, internal interference rejection, more robust front end architectures, and better tracking performance associated

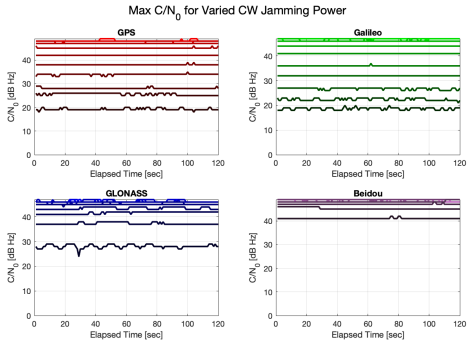

(a) u-blox receiver

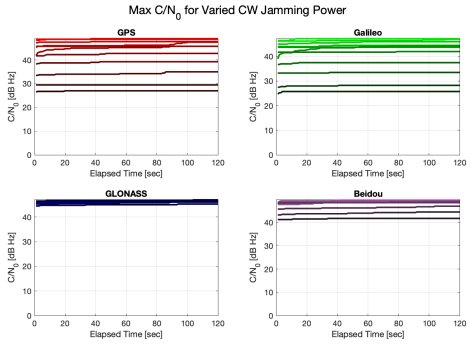

(b) Septentrio receiver

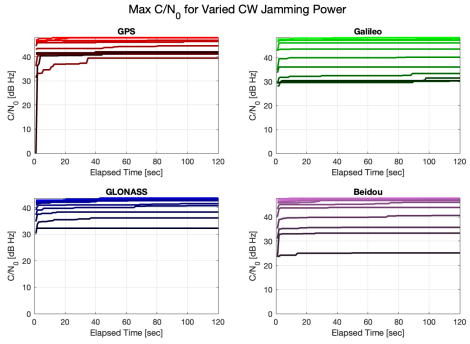

(c) Trimble receiver

Fig. 6: Comparison of maximum CN0 values across receivers (CW, u-blox antenna).

with those receivers.

The BeiDou and GLONASS signals show interesting behavior. Even though the BeiDou B1I and GLONASS L1 frequencies are not near the CW jamming frequency, drops are still observed across receiver types. The Septentrio receiver does a good job of filtering out the jamming from GLONASS, but the BeiDou CN0 still drops noticeably. The Trimble receiver records a drop in CN0 for both constellations. Some of this performance may be explained by the use of the antenna architecture as the cross-antenna comparisons explore this result in more detail.

The AGC data associated with the same CW jamming and u-blox antenna are in Fig. 7. The Trimble data files do not output the AGC, so only the u-blox and Septentrio measurements are included. The u-blox receiver records a single AGC value for the entire L1 band whereas the Septentrio records separate ones for each constellation's L1 signal. Overall drops in AGC are observed, except for the GLONASS L1 AGC which does not drop significantly, but does experience 2 dB drops and increased fluctuation. The smaller AGC drop for GLONASS is associated with the maintained CN0 values in Fig. 6b. In contrast, the decrease in CN0 for the other constellations accompanied an 18-20 dB drop in AGC.

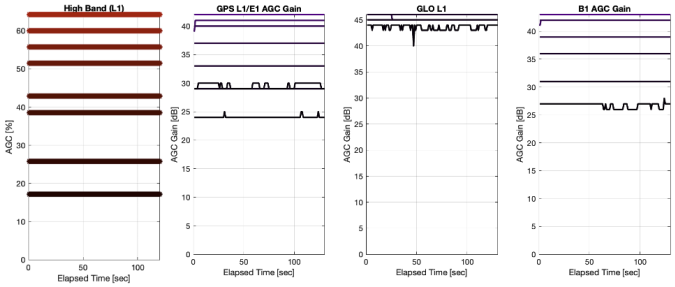

Fig. 7: Comparison of AGC values across receivers (CW, u-blox antenna)

For the second cross-receiver comparison, we compare the AWGN jamming results using the u-blox antenna. In Fig. 8, we see similar results between all three receivers, as all record 30 dBHz drops for GPS, Galileo, and BeiDou. This is reasonable because all three frequencies fall within the bandwidth of the prescribed jamming signal. The GLONASS signal only drops by 20 dBHz which is the result of the GLONASS L1 frequencies being distributed over a range, and the AWGN jamming signal only affecting the lower part of that range. As there will likely be a few GLONASS satellites that are not affected, the maximum CN0 plot will reflect these satellites and the jamming-affected satellites will not be reflected in the plot.

The AGC values for the AWGN jamming are included in Fig. 9. Discretized drops of 4-5 dB are observed for each constellation, with the BeiDou and GLONASS AGC values dropping an overall 10 dB less than for the GPS L1 AGC.

Third, we compare the CW jamming results using the Zephyr antenna in Fig. 10. These results using the survey-grade antenna show a clear improvement in CN0 values measured for the GLONASS and BeiDou constellations, compared to the u-blox antenna. Smaller overall drops in CN0 are observed with the Trimble receiver for GPS/Galileo. The u-blox and Septentrio receivers show no drop in GLONASS/BeiDou CN0, but a small drop of 10-12 dBHz is seen in the Trimble receiver.

The associated AGC results in Fig. 11 provide more detail into the CN0 series. For the Septentrio receiver, GLONASS AGC does not drop whereas the BeiDou AGC drops by 9 dB, even though the maximum CN0 values for both constellations do not drop.

Fourth, we compare the AWGN jamming results using the Zephyr antenna in Fig. 12. Similar to the previous case, the AWGN jamming affects GPS, Galileo and BeiDou signals

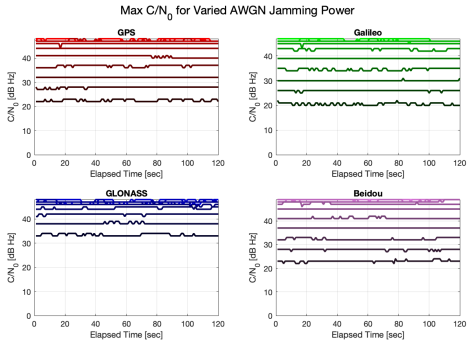

(a) u-blox receiver

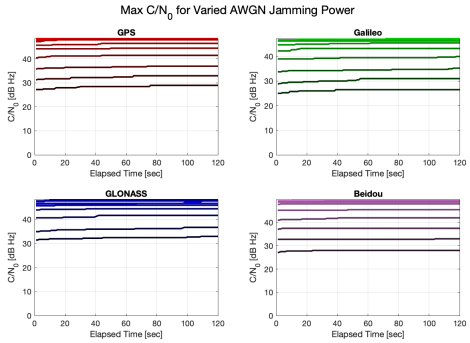

(b) Septentrio receiver

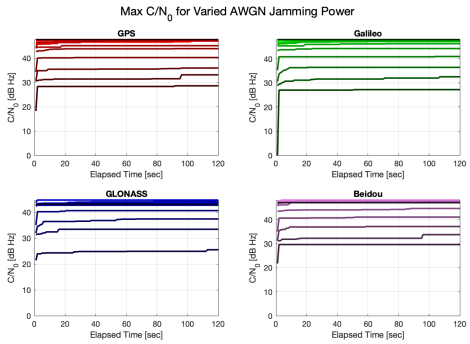

(c) Trimble receiver

Fig. 8: Comparison of maximum CN0 values across receivers (AWGN, u-blox antenna).

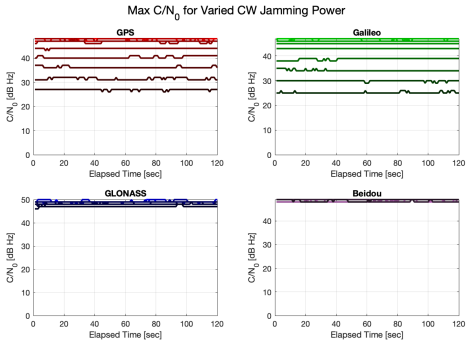

(a) u-blox receiver

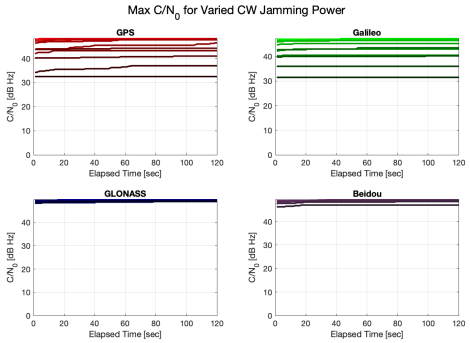

(b) Septentrio receiver

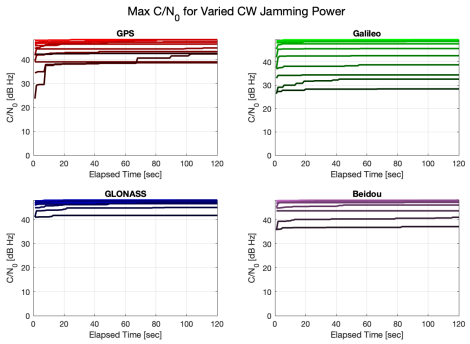

(c) Trimble receiver

Fig. 10: Comparison of maximum CN0 values across receivers (CW, Zephyr antenna).

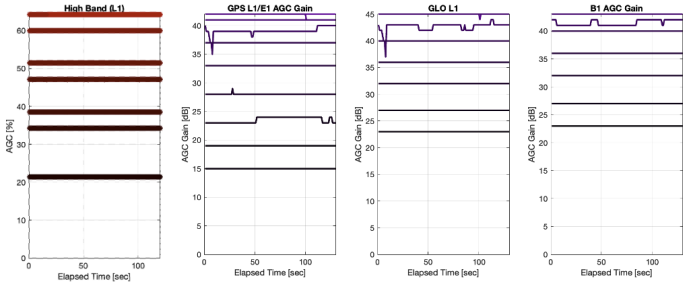

Fig. 9: Comparison of AGC values across receivers (AWGN, u-blox antenna)

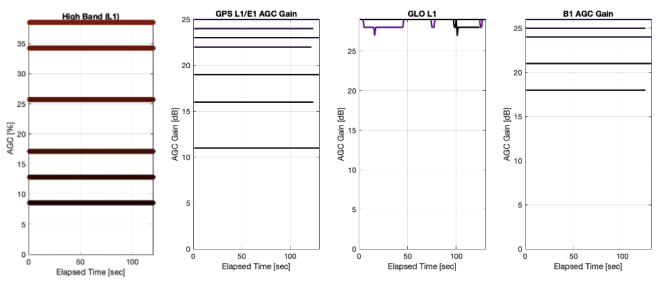

Fig. 11: Comparison of AGC values across receivers (CW, Zephyr antenna)

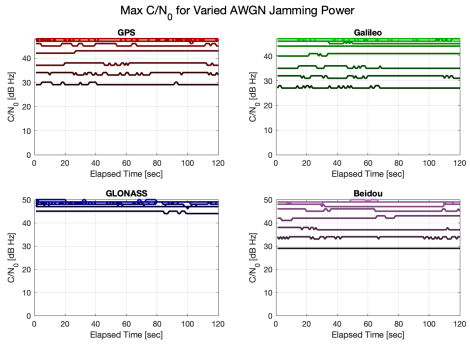

(a) u-blox receiver

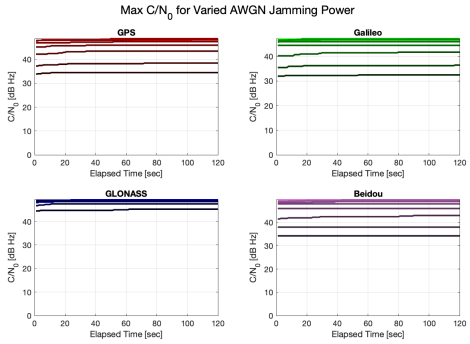

(b) Septentrio receiver

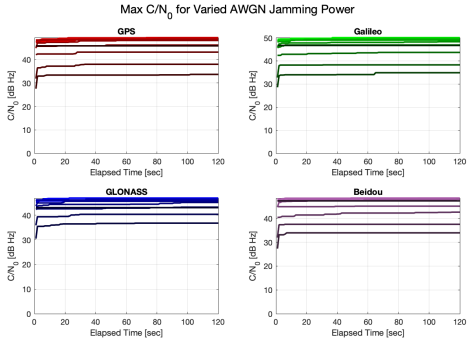

(c) Trimble receiver

Fig. 12: Comparison of maximum CN0 values across receivers (AWGN, Zephyr antenna).

significantly, and the GLONASS signals to a lesser extent. The GLONASS signal drops about 5 dBHz more for the Trimble measurements than for the u-blox and Septentrio measurements. This performance is further compared between antennas in the next section.

The associated AGC values are shown in Fig. 13. The noise jamming affects the AGC of all three frequencies, but it affects GLONASS AGC to a lesser extent as it only partially encroaches on the GLONASS L1 frequencies, and it affects BeiDou AGC almost as much as the AGC of the noise signal's center frequency at GPS L1.

Fifth, we look at the CW jamming results using the Sensor Systems antenna in Fig. 14. Here, the CN0 drops for GPS and Galileo are still significant, but are smaller for the Septentrio

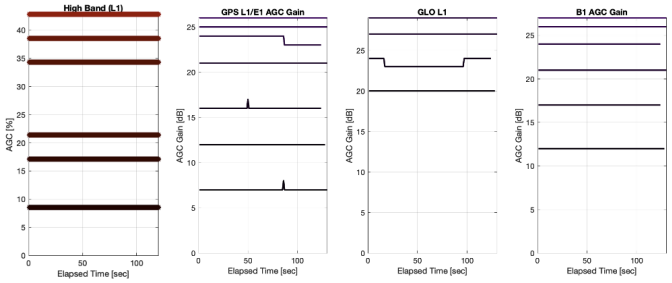

Fig. 13: Comparison of AGC values across receivers (AWGN, Zephyr antenna)

and Trimble receivers again. In this case, the BeiDou and GLONASS signals show no decrease at higher power across all receivers. This indicates that all three receivers were able to maintain the CN0 for these constellations and suggests that earlier observations might be the result of differences between antennas, which is explored in the next section.

The AGC results shown in Fig. 15 relatively small AGC drops associated with all signals, with a 7 dB drop for GPS L1/GAL E1, no drop for GLONASS L1, and a 4 dB drop for BeiDou B1I.

Finally, we look at the AWGN jamming results using the Sensor Systems antenna in Fig. 16. The results measured by the Septentrio and Trimble receivers are shown and show similar performance with slight 5 dBHz drops in BeiDou and GLONASS CN0 and slightly larger 7 dBHz drops for GPS and Galileo.

The associated AGC measurements are plotted in Fig. 17. They show relatively small decreases in AGC associated with higher levels of jamming power across all three frequencies.

Overall, the u-blox receiver consistently showed greater range in CN0 and AGC drops compared to the Septentrio and Trimble receivers. In the case of CW jamming, GPS and Galileo showed similar drops in maximum CN0 which were comparable across all three receivers; however, the GLONASS and BeiDou results varied. BeiDou maximum CN0 dropped by comparable amounts for the u-blox/Septentrio receivers and slightly more for the Trimble receiver in each CW jamming case. In general the GLONASS signals were less affected by the CW jamming though some Trimble measurements showed a slight drop. In the case of AWGN jamming, GLONASS and BeiDou signals were regularly affected and experienced CN0 drops slightly smaller than those for GPS and Galileo.

3) Cross-Antenna Comparison: To compare differences in measurements due to the antenna, the type of jamming and receiver are held constant.

The first comparison looks at data collected by the u-blox receiver with CW jamming. in Fig. 6a, Fig. 10a, and Fig. 14a for the u-blox, Zephyr, and Sensor Systems antennas, respectively. Overall, similar behavior was observed with GPS/GAL CN0 dropping 25 dBHz, 15 dBHz, and 11 dBHz, respectively. While the BeiDou and GLONASS signals did not drop for the survey and aviation antennas, there was a noticeable drop

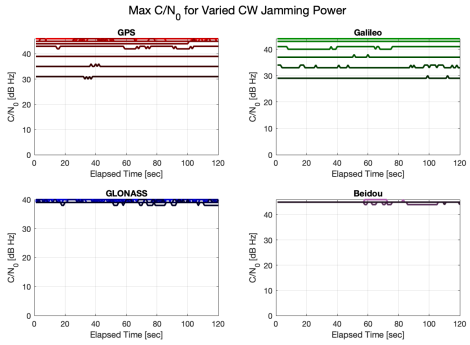

(a) u-blox receiver

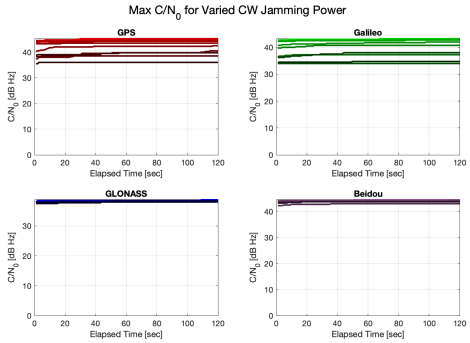

(b) Septentrio receiver

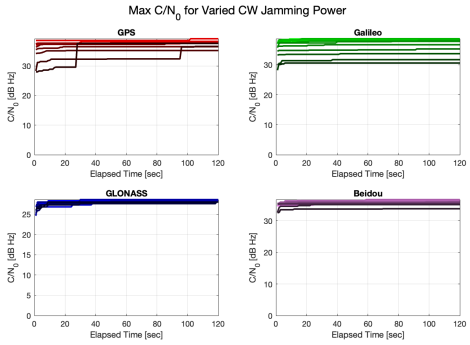

(c) Trimble receiver

Fig. 14: Comparison of maximum CN0 values across receivers (CW, Sensor Systems antenna).

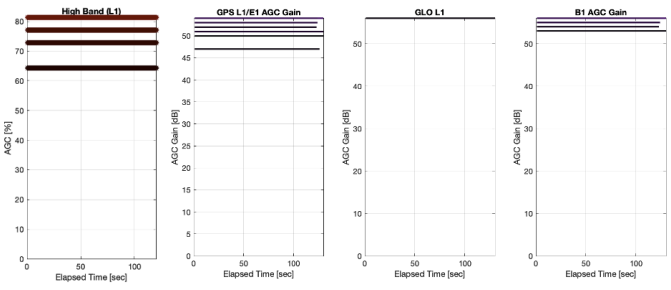

Fig. 15: Comparison of AGC values across receivers (CW, Sensor Systems antenna)

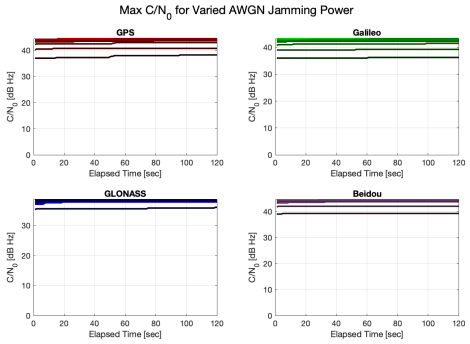

(a) Septentrio receiver

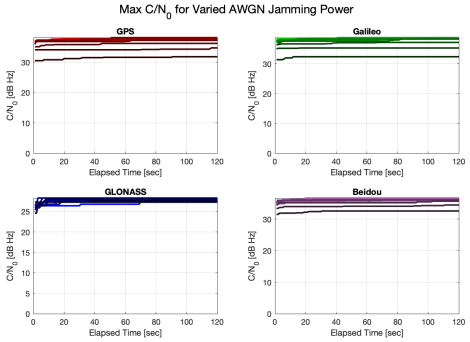

(b) Trimble receiver

Fig. 16: Comparison of maximum CN0 values across receivers (AWGN, Sensor Systems antenna).

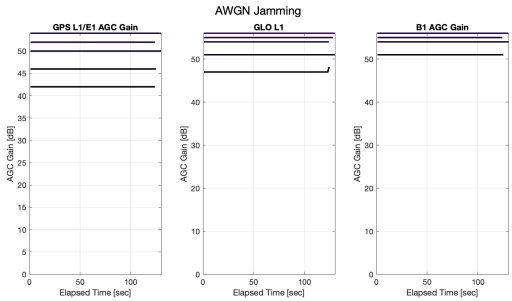

Fig. 17: Comparison of AGC values for the Septentrio receiver (AWGN, Sensor Systems antenna).

in CN0 for the u-blox antenna. Because these results come from the same receiver using different antennas, the effects observed are the results of the u-blox antenna.

The second comparison again looks at CW jamming but collected by the Septentrio receiver using different antennas. These results are shown in Fig. 6b, Fig. 10b, and Fig. 14b for the u-blox, Zephyr, and Sensor Systems antennas, respectively. With this receiver, the GPS/GAL results were similar for each case and CN0 dropped by smaller amounts with the Zephyr and Sensor Systems antennas. In all three cases, GLONASS is not significantly affected, and BeiDou only drops for the case with the u-blox antenna.

For a third comparison, we continue looking at the Septen-

trio receiver but with AWGN jamming, shown in shown in Fig. 8b, Fig. 12b, and Fig. 16a for the u-blox, Zephyr, and Sensor Systems antennas, respectively. The overall drop in CN0 for GPS/GAL is larger with the u-blox antenna and smaller with the Zephyr and Sensor Systems antennas. GLONASS shows significant drop in CN0 with the u-blox antenna, but not with the other antennas. BeiDou shows a larger CN0 drop with the u-blox antenna, but a smaller one with the Zephyr and a slight drop with the Sensor Systems antenna.

Overall, we see less of a dependence on antenna type in the AWGN case as the results are generally consistent between all three antenna types. Because all of the jamming is in-band, filtering out-of-band interference will not affect the metrics measured. This suggests the amplifiers along the path of the L1 signal might have an effect that would cause the drop in GLONASS and BeiDou for the CW jamming case.

GLONASS is unaffected by CW jamming except in the case of the u-blox antenna and u-blox receiver. BeiDou is generally unaffected by CW jamming except for slight drops in CN0 with the u-blox antenna. For AWGN jamming, GLONASS is slightly affected but is generally able to maintain the signal using the higher frequencies of the GLONASS L1 band that are outside the bandwidth of the AWGN signal. In the noise jamming case, BeiDou is generally affected nearly to the extent of GPS/GAL; however, differences in antenna architectures can mitigate the effect of the noise jamming on BeiDou signals an appreciable amount. Additionally, due to the different gains in each antenna, the magnitude of the starting AGC value is different in for each antenna, thought the size of drops in AGC are still the same.

4) Narrowband vs. Wideband Interference: Now, we compare the two jamming cases on the same receiver and antenna configuration. This section will highlight the differences in responses for narrowband or wideband jamming, which is important to consider when using receiver metrics to classify the type of RFI.

First, we compare the CW and AWGN cases for the u-blox antenna and the u-blox receiver. These results were shown in Fig. 6a and Fig. 8a. Immediately apparent is the larger drop in CN0 values for the BeiDou constellation in the AWGN case, compared to only slight drops in the CW jamming case. GLONASS experienced a similar drop in both cases.

Next, we compare the CW and AWGN cases for the u-blox antenna and the Septentrio receiver. First we look at the maximum CN0 values for each case, shown in Fig. 6b and Fig. 8b. Like the previous comparison, BeiDou signals are more affected by the AWGN jamming, but for the GLONASS signals are unaffected by the CW jamming and reasonably affected by the AWGN jamming, showing a 12 dBHz drop in CN0 compared to 20 dBHz drop in the other constellations. GPS/GAL are affected the same amount in both jamming cases.

More valuable for these comparisons is considering the AGC performance in these cases. The AGC for the receiver comparisons are shown in Fig. 7 and Fig. 9. For the CW jamming, the AGC for GPS L1/E1 dropping significantly while BeiDou B1I AGC drops by about 15 dB and GLONASS L1 AGC only drops by 4 dB. For the AWGN jamming, similar behavior is seen for GPS and BeiDou, but GLONASS AGC also decreases in this case.

The u-blox receiver has one AGC output for the L1 frequency band, meaning CW interference affecting GPS and Galileo may cause a decrease in L1 AGC, even though CN0 values for GLONASS and BeiDou may not have decreased. Across all cases tested, the decrease in a shared L1 AGC did not decrease the maximum CN0 of signals from constellations outside the range of the jamming signal.

Ultimately, CN0 and AGC decrease together in the presence of RFI with the magnitude of the drop being determined by the power of the RFI at a signal's frequency.

C. Metric-Power Level Relationship

The relationship between each metric and the jamming power level is seen in the previous comparisons; however, there is value in quantifying these relations. To quantitatively discuss these results, the data are presented again in a different format. The average of each maximum CN0 or AGC series is taken and plotted as a single point against the jamming power level associated with that series. The resulting plots are included below and visualize both the level at which performance degrades and provides a direct comparison between the rates of degradation for each configuration. The relationship between maximum CN0 and jamming power is shown for each configuration, with the cross-receiver comparison of AWGN/CW jamming for the u-blox antenna in Fig. 18 and Fig. 19, the cross-receiver comparison of AWGN/CW jamming for the Zephyr antenna in Fig. 20 and Fig. 21, and the cross-receiver comparison of AWGN/CW jamming for the u-blox antenna in Fig. 22 and Fig. 23. These each correspond with the associated figures in the previous section.

In each of these plots, the slope of the trendline is included in the legend. We see that the slope is generally steeper for frequencies that are more affected by interference, i.e. the GPS and GAL L1/E1 signals have steeper slopes in each case, while BeiDou B1I has a steeper slope in the AWGN jamming case compared to the CW jamming case. When plotting the relationship between metrics and power level, a linear trendline is fit to the decreasing data series using the MATLAB polyfit() function. As to not be influenced by nominal values at low power levels, the line is fit only to data points after the initial decrease in jamming power. The point at which the metrics decline is different in each configuration, so it is defined for the purpose of these plots as the first data point that is below the range of values observed in the nominal data run. In the case where there is not an observed decrease in CN0 or AGC values even at high jamming power, the trendline is simply fit to the whole series. For example, in Fig. 18a, the points considered in the trendline calculation are all those that fall below the range of nominal max CN0 values in the nominal data runs using the u-blox antenna/u-blox receiver configuration.

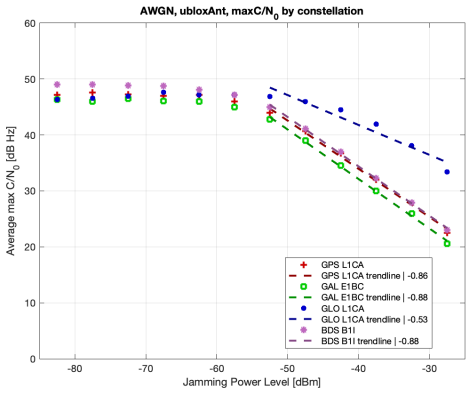

(a) u-blox receiver

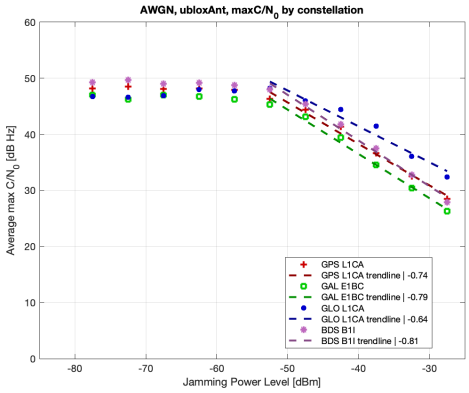

(b) Septentrio receiver

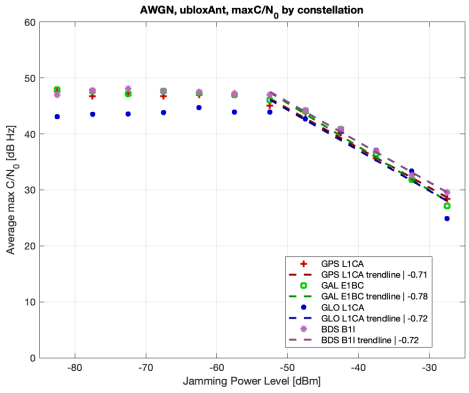

(c) Trimble receiver

Fig. 18: Cross-receiver comparison - Max. CN0 vs. Jamming Power (AWGN, u-blox antenna).

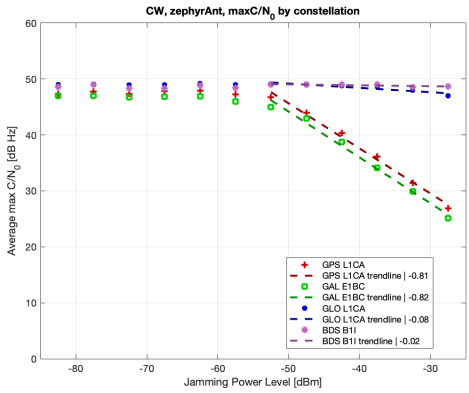

(a) u-blox receiver

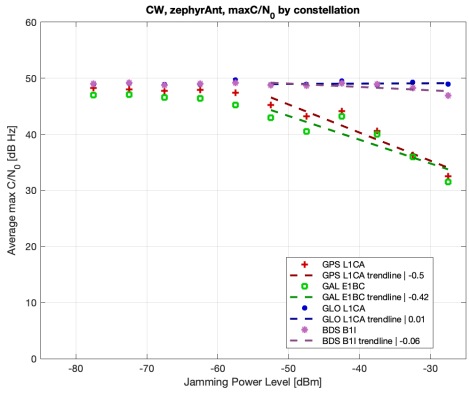

(b) Septentrio receiver

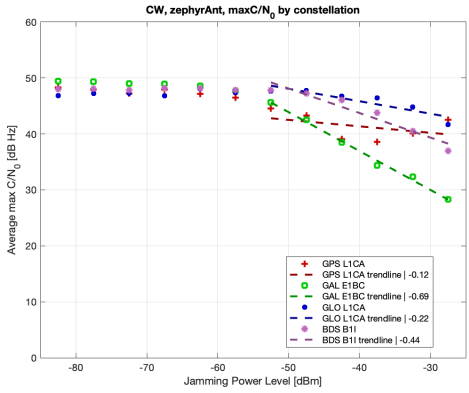

(c) Trimble receiver

Fig. 19: Cross-receiver comparison - Max. CN0 vs. Jamming Power (CW, u-blox antenna).

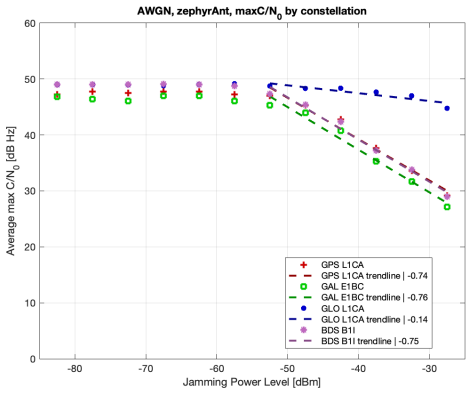

(a) u-blox receiver

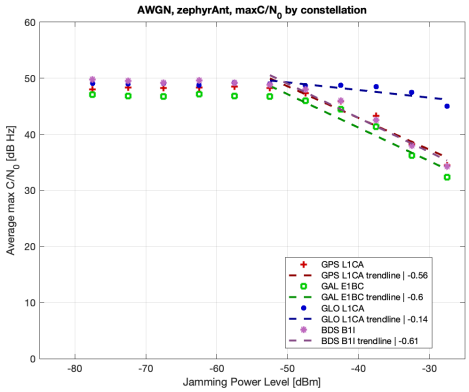

(b) Septentrio receiver

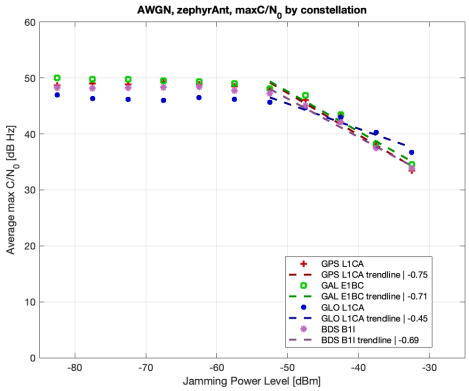

(c) Trimble receiver

Fig. 20: Cross-receiver comparison - Max. CN0 vs. Jamming Power (AWGN, Zephyr antenna).

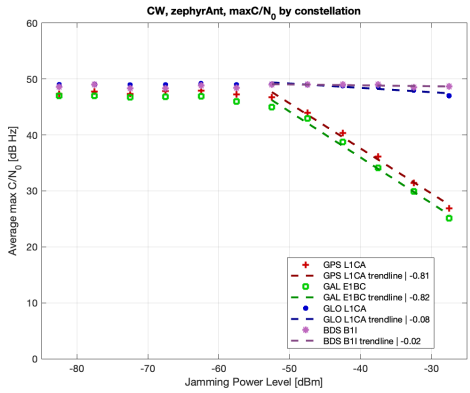

(a) u-blox receiver

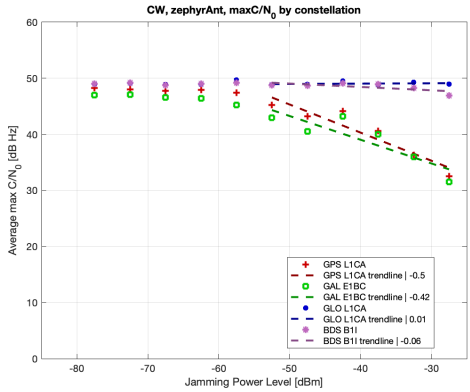

(b) Septentrio receiver

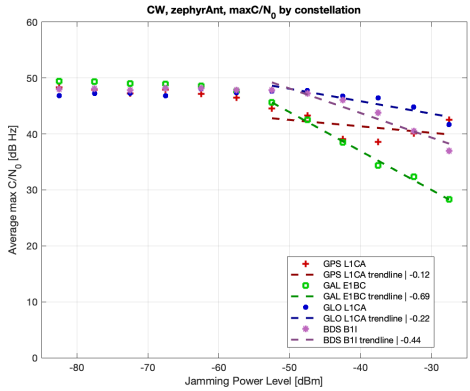

(c) Trimble receiver

Fig. 21: Cross-receiver comparison - Max. CN0 vs. Jamming Power (CW, Zephyr antenna).

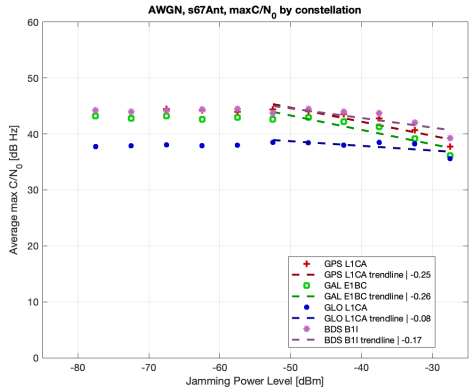

(a) Septentrio receiver

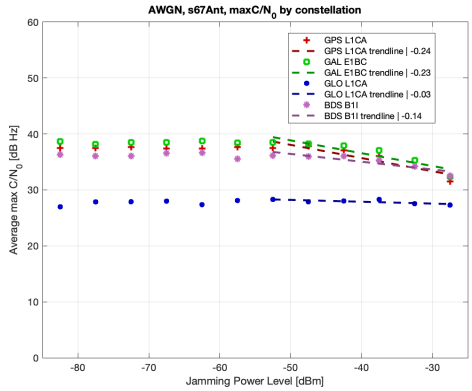

(b) Trimble receiver

Fig. 22: Cross-receiver comparison - Max. CN0 vs. Jamming Power (AWGN, Sensor Systems antenna).

Similarly, other metrics are plotted using this process. AGC and jamming power are related for each configuration as well. The results using the u-blox receiver as included in Fig. 24 for both jamming types. The AGC relationships from the Septentrio receiver are given in Fig. 25 and Fig. 26. These also correspond with the data shown in the AGC figures in the previous section.

These figures provide a quantitative summary of all the datasets collected and the relationships observed in each. When comparing the AGC relationships, the trendline slope varies by antenna in each scenario, and for a given antenna/receiver configuration, the slope is still associated with the degree to which a signal's frequency is affected by RFI. We see that for the u-blox receiver, a 1 dBm increase in jamming power corresponds with a >1 dB decrease in AGC whereas for the Septentrio receiver, the same increase corresponds to a <1dB AGC decrease. Thus, for the same jamming power, the Septentrio receiver is able to respond with a smaller change in front-end gain. The effect of this is that the Septentrio better minimizes subsequent quantization losses in the analog-to-digital converter and ultimately achieves better performance.

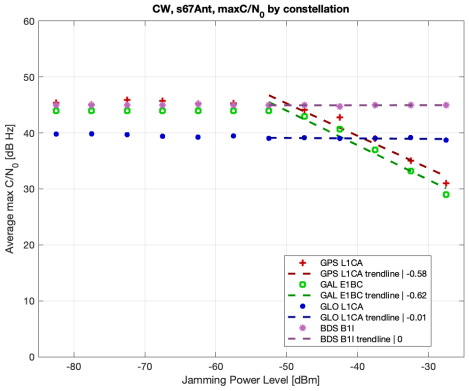

(a) u-blox receiver

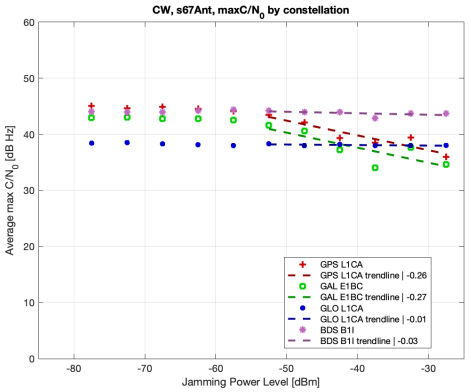

(b) Septentrio receiver

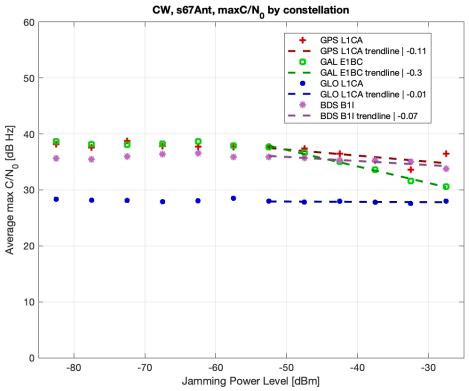

(c) Trimble receiver

Fig. 23: Cross-receiver comparison - Max. CN0 vs. Jamming Power (CW, Sensor Systems antenna).

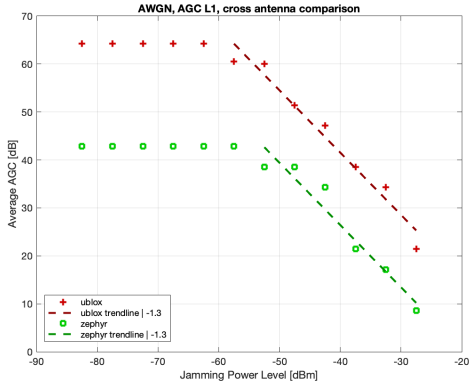

(a) AWGN jamming

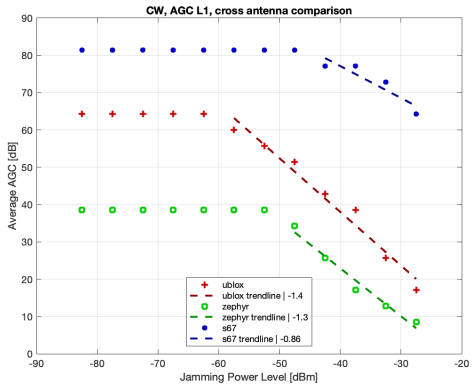

(b) CW Jamming

Fig. 24: Cross-antenna comparison - Average AGC vs. Jamming Power (u-blox receiver).

D. Thresholding

To interpret these metrics in a real-world setting, it is necessary to threshold these metrics to identify off-nominal states relative to a given nominal. These thresholds may be user-dependent, where stricter thresholds might be desired for safety-critical systems for example. The threshold value is a heuristic that can be set based on application-specific requirements. In the previous section, trendlines are calculated using only points that are off-nominal–that is, out of the range of CN0/AGC values collected in the nominal data series. Alternatively, a 2σ threshold may work well in general for nominal data that follows a normal distribution. However, more complex methods such as employing test statistics can be used too.

VI. Conclusions

The takeaways from this investigation are threefold. First, to develop a low-cost monitor, it is important to understand how an observed change in measurements corresponds to a change in RFI power. These relationships are tested and described quantitatively.

Second, measurements of interference detection metrics may change with different receiver implementations and differ-

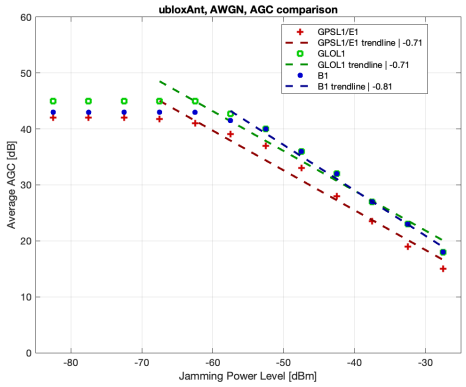

(a) u-blox Antenna

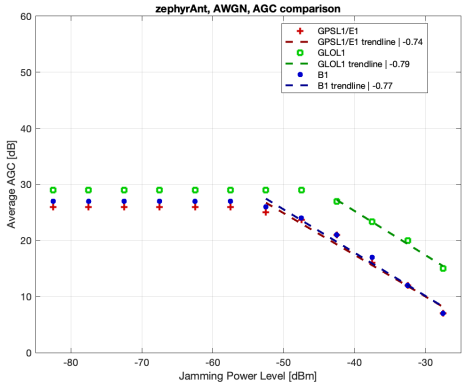

(b) Zephyr Antenna

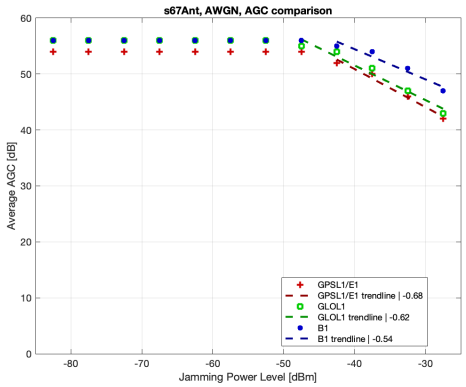

(c) Sensor Systems Antenna

Fig. 25: Average AGC vs. Jamming Power (AWGN, Septentrio receiver).

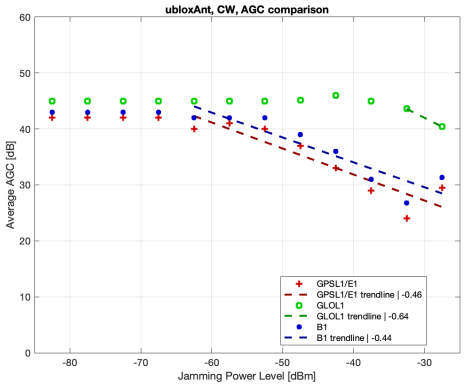

(a) u-blox Antenna

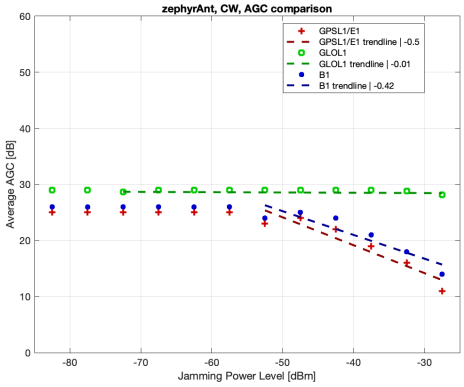

(b) Zephyr Antenna

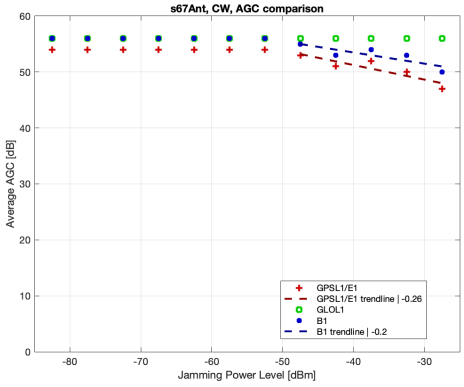

(c) Sensor Systems Antenna

Fig. 26: Average AGC vs. Jamming Power (CW, Septentrio receiver).

ent antennas. When designing a network of low-cost receivers, antenna architectures and receiver characteristics should be considered accordingly, as the choice of an antenna and receiver can significantly affect measurements.

Third, there is a tradeoff between sensitivity and robustness against RFI with low-cost and expensive receivers. Low-cost receivers have greater sensitivity to CN0 and AGC drops, but this provides greater resolution to describe RFI at that state. In contrast, an expensive receiver may have built-in RFI resilience that results in metrics that only drop slightly with strong RFI. This provides little resolution to identify, classify, or locate the interference. Provided a user can maintain a position using low-cost receivers in the presence of some RFI, a low-cost network setup will provide more resolution into understanding the state of RFI.

For future development of a low-cost monitor, understanding how different interference levels affect our receiver helps us to set the appropriate threshold for when to warn the user of the presence of RFI. Too many warnings for low levels of interference will result in users disregarding the alert. While delaying the alert until too late is also not useful. These calibrations are essential to identifying the most useful ranges for when to declare the presence of harmful RFI.

ACKNOWLEDGMENT

We gratefully acknowledge the support of The Aerospace Corporation under their University Partnership Program and the Federal Aviation Administration for supporting this effort.

REFERENCES

[1] D. Goward, “DHS Report on Denver Jamming – More questions than answers,” GPS World, Jan. 2023. Accessed: Apr. 24, 2023. [Online].

[2] D. Goodin, “GPS interference caused the FAA to reroute Texas air traffic. Experts stumped,” ARS Technica, Oct. 2022. Accessed: Apr. 24, 2023. [Online].

[3] S. Henn, “Could The New Air Traffic Control System Be Hacked?,” ARS Technica, Oct. 2022. Accessed: Apr. 24, 2023. [Online].

[4] L. Taleghani, F. Rothmaier, Y-H. Chen, S. Lo, T. Walter, D. Akos, and B. Granite Gattis, “Low cost RFI monitor for continuous observation and characterization of localized interference sources,” Published in Proceedings of the 2022 International Technical Meeting of The Institute of Navigation, Long Beach, CA, January 2022.

[5] N. San Miguel, Y-H. Chen, S. Lo, T. Walter, and D. Akos, “Stress testing of a low-cost GNSS RFI monitor,” Published in Proceedings of the 35th International Technical Meeting of The Satellite Division of the Institute of Navigation (ION GNSS+ 2022), Denver, CO, September 2022.

[6] J. R. van der Merwe et al., “Low-Cost COTS GNSS Interference Monitoring, Detection, and Classification System,” Sensors, vol. 23, no. 7, p. 3452, Mar. 2023, doi: 10.3390/s23073452.

[7] J. Lindström, D. Akos, O. Isoz, and M. Junered, “GNSS interference detection and localization using a network of low cost front-end modules,” Proceedings of the 20th International Technical Meeting of The Satellite Division of the Institute of Navigation (ION GNSS+ 2007), Fort Worth, TX, September 2007.

[8] F. Bastide, D. Akos, C. Macabiau, B. Roturier, “Automatic gain control (AGC) as an interference assessment tool,” Proceedings of the 16th International Technical Meeting of the Satellite Division of The Institute of Navigation (ION GPS/GNSS 2003), Portland, OR, September 2003, pp. 2042-2053.

[9] P. W. Ward, “What’s Going On? RFI Situational Awareness in GNSS Receivers,” InsideGNSS, Sep. 2007. Accessed: Apr. 27, 2023. [Online].

[10] K. Gromov, D. Akos, S. Pullen, P. Enge, and B. Parkinson, "GIDL: generalized interference detection and localization system," Published in Proceedings of the 13th International Technical Meeting of The Satellite Division of the Institute of Navigation (ION GPS 2000), Salt Lake City, UT, September 2000.
[11] F. Rothmaier, Y. -H. Chen, S. Lo and T. Walter, "A Framework for GNSS Spoofing Detection Through Combinations of Metrics," in IEEE Transactions on Aerospace and Electronic Systems, vol. 57, no. 6, pp. 3633-3647, Dec. 2021, doi: 10.1109/TAES.2021.3082673.
[12] u-blox, "u-blox ZED-F9P Interface Description - Manual," F9P-10B Interface Description, Jul. 2019 [Accessed April 2023]
[13] Septentrio NV, "mosaic-X5 Reference Guide," mosaic-X5 Reference Guide, Apr. 2022 [Accessed April 2023]
[14] Trimble, "Trimble BX940 - GNSS solutions for oems - triple-frequency receiver, rugged enclosure," BX940 Reference Guide, Jul. 2021 [Accessed Apr. 2023]
[15] u-blox, "ANN-MB1 L1/L5 multi-band high precision GNSS antenna Datasheet," ANN-MB1 Data sheet, Nov. 2022.
[16] Trimble, "Trimble Zephyr 2 Antennas Datasheet," Zephyr 2 Geodetic Data sheet, Jan. 2017.
[17] Sensor Systems Inc., "GPS S67-1575-175: L1/L5 Datasheet," GPS L1/L5 antenna data sheet, Sep. 2016.
[18] Akos, D. M., "Who's Afraid of the Spoofer? GPS/GNSS Spoofing Detection via Automatic Gain Control (AGC)," NAVIGATION, Journal of the Institute of Navigation, vol. 59, no. 4, pp. 281–290, 2012.